Jamming analysis on the behaviours of liquefied sand and virgin sand subject to monotonic undrained shearing

Jamming analysis on the behaviours of liquefied sand and virgin sand subject to monotonic undrained shearing

Xin Huang[a,b*], Kevin J. Hanley[c], Zixin Zhang[a,b], Chungyee Kwok[d], Mingze Xu[a,b]

[a] Key Laboratory of Geotechnical and Underground Engineering, Ministry of Education, Tongji University, 1239 Siping Road, Shanghai 200092, China

[b] Department of Geotechnical Engineering, Tongji University, 1239 Siping Road, Shanghai 200092, China

[c] School of Engineering, Institute for Infrastructure and Environment, The University of Edinburgh, Edinburgh EH9 3JL, United Kingdom

[d] Department of Civil Engineering, The University of Hong Kong, Pokfulam Road, Hong Kong, China

*Corresponding author: xhuang@tongji.edu.cn

Declarations of interest: none

Abstract

It is well documented in the experimental literature that liquefied sands behave differently from virgin sands without a shearing history. In this study, undrained DEM simulations were performed on both a virgin sample and samples liquefied by cyclic loading. An identical critical state was reached regardless of liquefaction history. The fundamental mechanisms underlying the difference in the stress–strain responses between the liquefied sands and virgin sand were interpreted within the framework of jamming transition. The virgin sample was jammed throughout the simulation, characterised by a fully-percolated force transmission network of increasing resilience and mechanical stability. In contrast, the initially liquefied samples experienced an apparent phase transition from unjammed to jammed states. A fully-percolated force transmission network did not exist, and thus the unjammed samples flowed during the initial stage of loading. As loading proceeded, the force transmission network became fully percolated, and its resilience and mechanical stability developed. All of the micro-scale parameters reflecting the resilience and mechanical stability of the force transmission network reached identical values at the critical state independent of liquefaction history. Finally, a micro-scale approach based on the degree of indeterminacy was proposed to identify the four-stage post-liquefaction behaviour.

Keywords: Liquefaction; jamming transition; resilience; mechanical redundancy

1 Introduction

Earthquakes are one of the most devastating natural hazards that threaten the lives and possessions of human beings. The damage to structures and pipelines caused by seismic loading is mainly attributed to soil liquefaction, which is characterised by a complete loss of soil strength and stiffness [1]. Previous studies of soil liquefaction have principally focused on two aspects: liquefaction potential and countermeasures against the occurrence of liquefaction. However, a comprehensive knowledge of post-liquefaction behaviour is also of great importance to geotechnical engineers as it is closely related to the liquefaction–induced deformations and displacements [2]. Moreover, it permits safety and serviceability assessment of structures surviving after an earthquake and guides the design of reconstruction projects on/in the liquefied ground.

Experimental studies have revealed that liquefied sands behave considerably differently from virgin sands [3-8]. Virgin sand may exhibit flow liquefaction, limited liquefaction or strain-hardening subjected to undrained monotonic triaxial loading depending on the initial packing density and confining pressure. However, the stress–strain behaviour of liquefied sands subjected to undrained triaxial loading typically involves three stages regardless of packing density (see Fig. 1). Phase I is the fluidic stage, during which the stiffness is essentially close to zero and the deformation develops quickly with negligible soil strength. In phase II, soil gradually mobilises its strength and the modulus increases with increasing strain. In phase III, soil continues to mobilise its strength with an approximately constant modulus. Within the framework of critical state soil mechanics (CSSM) [9], one may also expect a Phase IV, i.e., a steady state where the soil deforms continuously under constant stress and constant volume. This, however, has rarely been reported in laboratory tests due to equipment limitations and high non-uniformity of stress or deformation [8]. In addition to laboratory tests, some work has been done to constitutively model the post-liquefaction behaviour [10-12] and the three-stage characteristics of liquefied sand have also been confirmed in discrete element simulations [7]. However, there are still two questions related to the fundamentals of the mechanical behaviour of liquefied sand that need further exploration: *a) why does liquefied sand behave differently from virgin sand subjected to the same loading condition? b)*

what is the fundamental mechanism underlying the recovery process of strength and stiffness of liquefied sand? Since sand is a typical granular material whose macroscopic responses are governed by grain-scale movements and grain-to-grain interactions, answering these two questions requires insightful exploration at the particulate level.

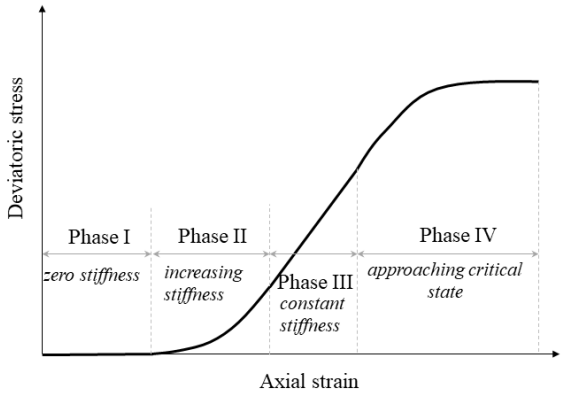

Figure 1 Schematic illustration of the typical stress–strain responses of liquefied sand subjected to undrained triaxial compression (modified from [8])

Within the physics community, much effort has been devoted to investigating the jamming transition of granular materials [13-17]. Liu & Nagel [13] distinguish two phases: a) unjammed phase (fluid-like), in which the granular system flows under any applied stresses; b) jammed phase (solid-like), in which the granular system can resist small stresses without deforming irreversibly. Cates et al. [18] proposed that there exists a crossover – a fragile state – in which a granular system can only sustain loads compatible with its current force-bearing network and will experience significant plastic particle arrangement if the loads deviate from the original compression axis. Pouragha & Wan [19] made the advance of linking the concepts of jamming and critical state in soil mechanics based on the principle of mechanical redundancy. Liquefaction is a process during which sand gradually loses its strength and stiffness, which causes sand to evolve from a solid state to a flow state. This is essentially analogous to the process from a jammed state to an unjammed state. Therefore, it is an intuitive idea that the regaining of strength and stiffness of liquefied soils should be the reverse of this process, i.e., a transition from unjamming to jamming. This will be explored in the current paper.

The discrete element method (DEM) originally proposed by Cundall & Strack [20] has been used across a wide range of disciplines, including civil engineering, chemistry, physics and bioscience [21]. It is well documented that DEM is capable of capturing the mechanical behaviour of soils ranging from the small- to large-strain levels under both static and dynamic loading conditions [22-28]. Wang & Wei [29] found that the Mean Neighboring Particle Distance (MNPD) they proposed has the best correlation with the post-liquefaction shear strain development based on DEM simulations. Wei et al. [30] proposed two void-based fabric indices to quantify the anisotropy of local void distribution, based on which a unique hardening line that separates flow and jamming states was identified. Furthermore, DEM simulations can provide comprehensive particle-scale information that is difficult to access in physical laboratory tests, which provides insights into the fundamental mechanisms that underlie the complex macro-scale soil behaviour.

This paper attempts to answer the two questions identified above from a microscopic perspective. A series of constant-volume DEM simulations were performed on both virgin samples and samples which have liquefied during cyclic loading. The difference between virgin and liquefied sands in their mechanical behaviour and the recovery process of stress and stiffness of liquefied sands upon monotonic shearing were explained within the framework of jamming transition through the analyses of percolation, resilience of force transmission networks and mechanical redundancy. This is the main novelty of this paper, enabling the proposal of a rational, micro-scale approach based on mechanical stability to distinguish the different phases of post-liquefaction behaviour, including the fourth phase: critical state.

2 Overview of DEM simulations

Simulations were performed using the well-recognised commercial software PFC3D [31]. A DEM sample containing 19449 unbreakable spherical particles was created within a cylindrical space enclosed by rigid walls. As shown in Fig. 2, the grading of Toyoura sand is approximated, which is a moderate polydisperse system with a size span (difference between

the maximum and minimum particle diameters/sum of the maximum and minimum particle diameters) of 0.56.

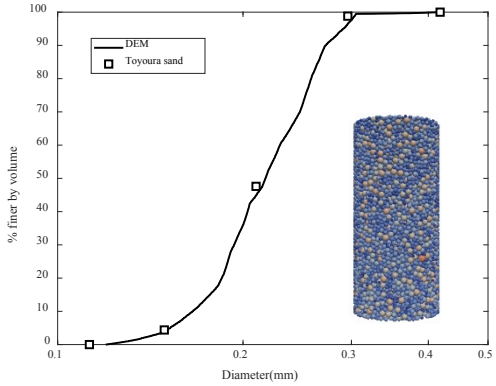

Figure 2 Comparison between the experimental grading curve and the numerical grading curve

Particles were firstly generated at half of their required sizes without contacting each other within a cylindrical space bounded by frictionless rigid walls, and then were gradually expanded to their target sizes. The assembly was compressed isotropically until a mean stress of 500 *kPa* was reached. A simplified Hertz-Mindlin model is adopted with a particle shear modulus of 29 *GPa* and a particle Poisson's ratio of 0.12 [25]. Gravity is neglected in the current study. During isotropic compression, the interparticle friction coefficient (μ) was set to be 0.3 to get a void ratio of 0.697. μ was then increased to 0.5 and the system was numerically cycled to an equilibrium state before shearing commenced. A local damping mechanism was adopted with a damping ratio of 0.1. After isotropic compression, the sample was firstly subjected to cyclic shearing, during which the deviatoric stress (q) followed a sinusoidal variation (Eq. 1) while the boundary positions were adjusted continuously at the same time to maintain a constant-volume condition:

$$q = q_{cyc}\sin(\omega t) \qquad \text{(Eq. 1)}$$

in which q_{cyc} is the cyclic stress amplitude, 200 *kPa*, and ω is the cyclic loading angular frequency which was selected as 10 *Hz*. Fig. 3(a) shows the evolution of deviatoric stress, q, and the excess pore water pressure, u, with the number of loading cycles for this one simulation which liquefied multiple times. Fig. 3(b) plots q against the axial strain, ε_a. The

excess pore water pressure, u, has been computed as the difference between the initial confining pressure and the mean effective stress, p'. Cyclic mobility, which is typical for medium dense sands, is observed: liquefaction is initiated at around the 12.5th loading cycle and recurs at the 13th, 13.5th and 14th loading cycles. The samples at the selected liquefied instants, shown by the pairs of circular markers on Fig. 3(a) and 3(b), were then subjected to constant-volume monotonic triaxial shearing by applying an axial strain rate of 1 s^{-1}. For comparison, constant-volume monotonic shearing was also performed on the virgin sample generated after isotropic compression with no shearing history. Details of the selected liquefaction instants are given in Table 1. Note that PL in the sample ID indicates 'post-liquefaction'. The initial residual axial strain corresponds to the residual axial strain generated during cyclic loading at selected instants ① to ④ as shown in Fig. 3(b). These axial strains were generated prior to the monotonic constant-volume simulations discussed in Sec. 4, and thus are called 'initial residual axial strains' to distinguish them from the axial strains generated during the successive monotonic loading simulations.

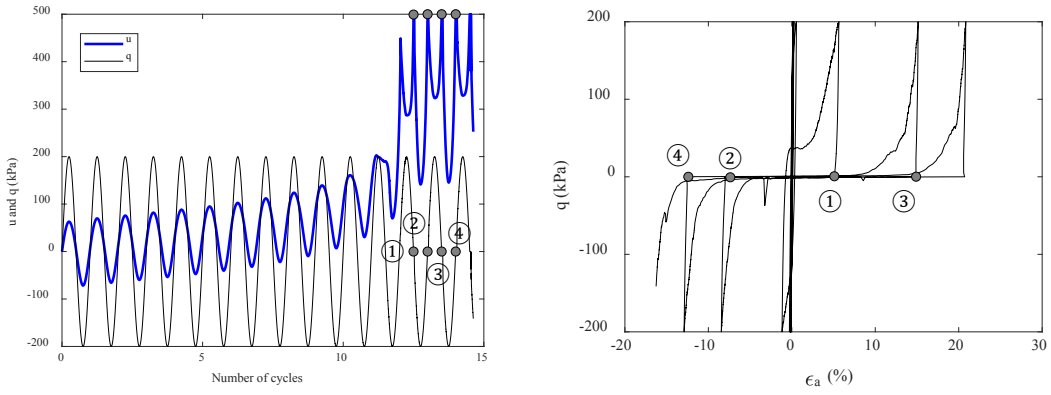

(a) (b)

Figure 3 Stress–strain behaviour during cyclic loading for a single simulation in which the circular markers denote instants at which liquefaction occurs

Table 1 Information of the selected simulation instants coinciding with liquefaction

ID	Cycle Number to Liquefaction	Initial residual axial strain, $\varepsilon_{a,0}$ (%)
PL-1	12.5	5.097
PL-2	13	-7.368

PL-3	13.5	13.92
PL-4	14	-12.69

3 Results and discussion

3.1 Stress–strain response

Figure 4 shows the post-liquefaction stress–strain behaviour for the four simulations which take the instants listed in Table 1 as the starting states for constant-volume monotonic shearing. The stress–strain behaviour of the virgin sample is overlaid for comparison. For the four post-liquefaction samples, the typical four-stage post-liquefaction behaviour of sands can be clearly seen, in line with experimental observations. At the first stage, the deviatoric stress (q) remains close to zero but the axial strain (ε_a) develops considerably, i.e., the samples behave essentially like a liquid with no stiffness. At the second stage, the deviatoric stress starts to grow with the axial strain at an increasing rate. The deviatoric stress continues to increase but the stiffness remains approximately constant at the third stage. Finally, the rate of increase of the deviatoric stress gradually reduces until the critical state is reached. The post-liquefaction axial strains (ε_a-$\varepsilon_{a,0}$) at which q reaches 5 *kPa* are 1.134%, 20.07%, 1.435%, 32.136% for PL-1 to PL-4, respectively. This 5 *kPa* criterion was proposed by Vaid & Thomas [4] to distinguish Phases I and II. Distinguishing the other three phases is somewhat subjective and thus is not discussed here. A larger deformation is needed for PL samples with extensive residual strains (PL-2 and PL-4) to regain strength than for PL samples with compressive residual strains (PL-1 and PL-3). The post-liquefaction axial strains of Phase I are obviously smaller for PL-1 and PL-3 originally with compressive residual strains in comparison to those for PL-2 and PL-4 originally with extensive residual strains. The curves of Phase III for the four post-liquefaction simulations are almost parallel to each other and have a slope (stiffness) that is close to (slightly smaller than) that of the virgin sand, agreeing with experimental findings. It should be noted that the liquefied samples experienced a larger axial strain than the virgin sample before reaching the critical state. This may be because the initial loading–unloading cycles during cyclic loading caused the force transmission network to disintegrate and the particles were in a flowing state in the liquefied samples. When

subjected to shearing, the axial strain developed rapidly. As shown in Fig. 4(a), a large proportion of the strains occurred during Phase I, when the liquefied samples behaved like a liquid. Once a percolated force network had been formed, the liquefied samples regained rigidity and development of axial strain was greatly slowed down (see Section 3.3).

As Fig. 4(b) shows, the stress paths for the four post-liquefaction samples coincide with each other, following a linear trend. The slope of the post-liquefaction simulation curves is slightly larger than for the virgin sample at low stress but becomes almost identical to that of the virgin sample when the critical state is reached. An interesting finding is that all five simulations, including the virgin sample, reach an identical critical state, which indicates that the critical state does not depend on the liquefaction history. The q values at the critical state reach around 20 *MPa*. This is due to the use of a nonlinear Hertz-Mindlin contact model which indicates increasing contact stiffnesses with increasing particle–particle overlapping and the absence of any particle crushing mechanism. In reality, sand grains are likely to crush and their asperities are likely to yield subject to such a high level of stress. As noted by Hanley et al. [32], the critical-state stresses can be greatly reduced when particle crushing is considered.

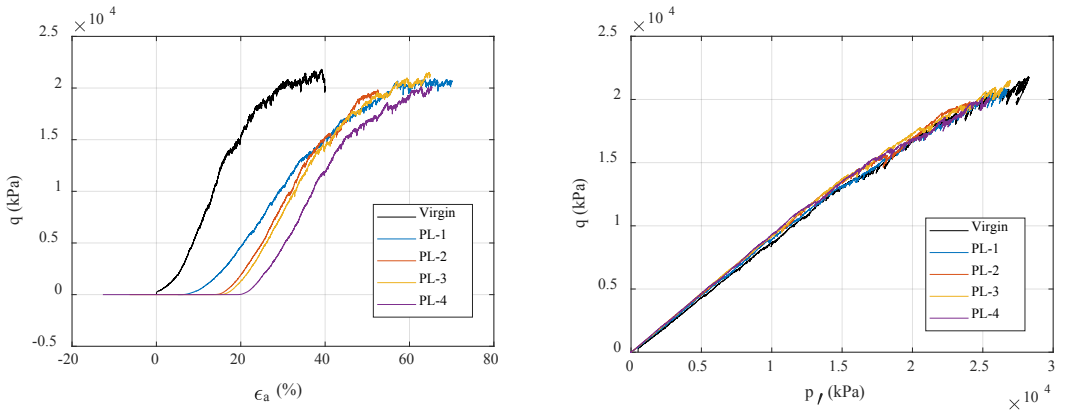

(a) (b)

Figure 4 Stress–strain behaviour of liquefied samples and the virgin sample during constant-volume simulations: (a) q–ε_a; (b) stress path. ε_a here for each post-liquefaction sample starts from $\varepsilon_{a,0}$ shown in Table 1.

3.2 Inertia effect

da Cruz et al. [33] proposed a rheological model for dense granular flows based on the inertia number,

$$I = \dot{\varepsilon} d \sqrt{\rho / p'} \qquad \text{(Eq. 2)}$$

where $\dot{\varepsilon}$ is the shear rate, d is the mean particle size of the assembly, ρ is the grain density and p' is the mean effective stress. They divided the dense granular flow into a quasi-static regime with low I values, a collisional flow regime with high I values and an intermediate dense flow regime. In the collisional flow regime, particles are of high kinetic energy, and thus instantaneous uncorrelated collisions between particles dominate. In this regime, the contacts are mostly short-lived and deformation can be large subject to infinitesimal deviatoric loads. In the quasi-static regime, the external loads are mainly transmitted by a well-percolated force transmission network. The sample behaves like a solid with some rigidity; thereby, the sample can sustain a certain amount of deviatoric load without significant deformation. These two mechanisms coexist in the intermediate dense flow regime. The evolution of inertia number in the current simulations is presented in Fig. 5. Since the threshold I values separating the quasi-static regime from the dense flow regime and separating the dense flow regime from the collisional flow regime depend on many factors, including the sample size and particle size distributions [33-34], it is difficult to exactly distinguish the three different regimes. However, some qualitative observations are apparent. For the virgin sample, the inertia number maintained at a very small value and continued to decrease during loading due to the increasing stability of the force transmission network, i.e., quasi-static shearing was persistent throughout the simulation. A clear transition from a collisional flow state to a quasi-static shear state could be identified for the liquefied samples. The liquefied samples were initially in a flow state characterised by high inertia numbers. The inertia number decreased sharply during loading and the samples gradually changed from a collisional flow state to a quasi-static state as the inertia number further increased; during this period the deformation developed rapidly but the deviatoric stress remained negligible (see the horizontal curves in Fig. 4(a)). Once the sample entered the quasi-static regime, the sample started to attain some rigidity. Consequently, as Fig. 4 shows, the rate of deformation

development greatly slowed down and the deviatoric stress increased notably. This is the fundamental mechanism of post-liquefaction behaviour interpreted by the variation of inertia number.

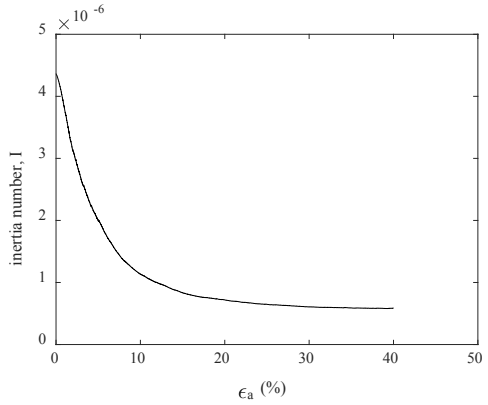

(a) Virgin sample

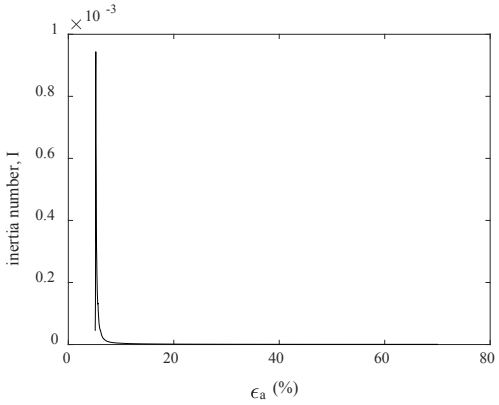

(b) PL-1

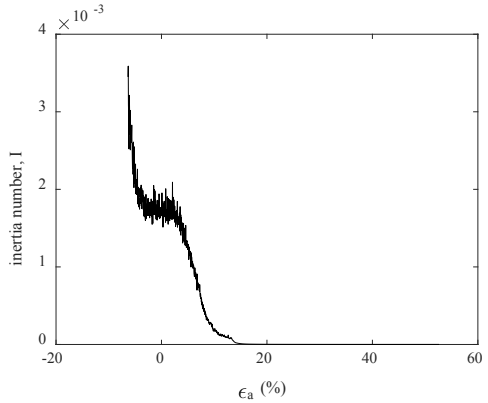

(c) PL-2

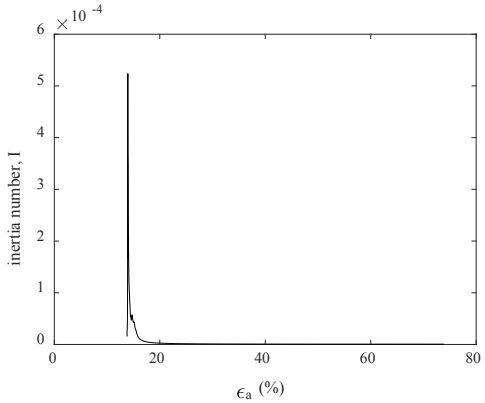

(d) PL-3

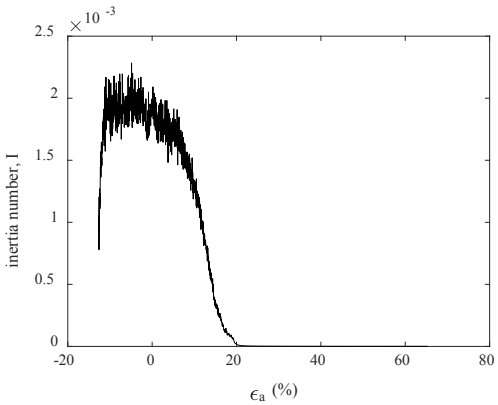

(e) PL-4

Figure 5 Evolution of inertia number during triaxial shearing

3.3 Percolation analysis

Percolation analysis was first used by Bi et al. [16] to identify different phases in the process of unjamming–jamming or jamming–unjamming transitions. Different phases can be identified based on the percolation index which is defined as the ratio of the largest force transmission network (ξ_i) in all dimensions to the corresponding dimensions (L_i) of the analysis domain, i.e., ξ_i / L_i (i = 1, 2 in 2D and 1, 2 or 3 in 3D). Specifically, the largest force transmission network is defined herein as the force transmission network containing the largest number of particles and the analysis domain corresponds to the entire sample. A 2D illustration of the definitions of different phases based on the percolation index is shown in Fig. 6. When the force transmission network percolates in all dimensions ($\xi_i / L_i \approx 1$ for all i), the sample is in a jammed state and behaves similarly to a solid (Fig. 6(a)); when the force transmission network percolates in at least one but fewer than i dimensions, the sample is in a fragile state (Fig. 6(b)); when the force transmission network does not percolate in any direction, the sample is in an unjammed state and flow occurs (Fig. 6(c)).

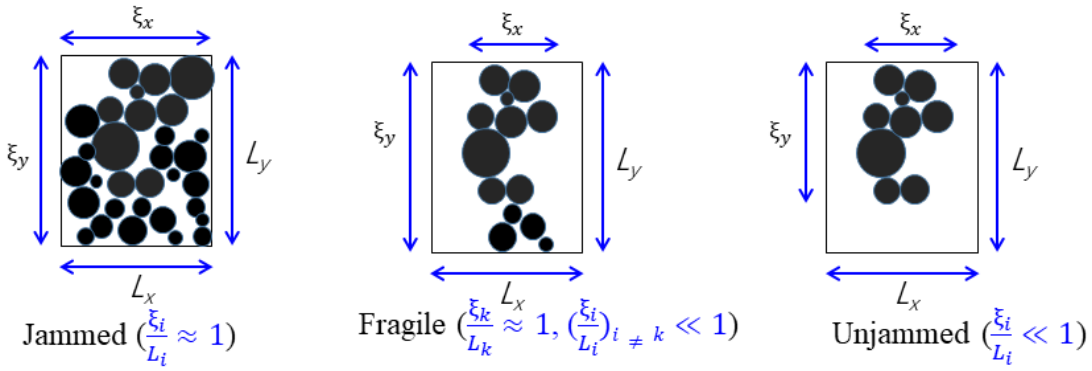

(a) (b) (c)

Figure 6 Definitions of different phases based on percolation analysis. Black particles are components of the largest force transmission network

ξ_i is obtained in a multi-step process. Firstly, clusters, i.e., groups of interconnected particles, are identified. A single particle is selected and its contacting neighbours are identified by

parsing the neighbour list. The same procedure is applied recursively to all of these contacting particles until all of the particles comprising the cluster have been identified. Other clusters are identified by starting this procedure from particles not already members of a cluster. After all particles have been either associated with a cluster or found to be isolated particles, the cluster containing the most particles is the major force transmission network. ξ_i is the difference between the upper and lower bounding coordinates of this major force transmission network.

Fig. 7 shows the percolation analysis results of the five simulations presented in Fig. 4. The vertical dashed lines mark the end of Phase I, at which the deviatoric stress exceeds 5 *kPa*, for the four post-liquefied samples. For ease of comparison, the strains shown in Fig. 7 and subsequent figures are purely the axial strains (ε_a-$\varepsilon_{a,0}$) developed during the post-liquefaction simulations. For the virgin sand, the percolation indexes are all close to 1 throughout the simulation, which indicates that the sample is consistently in a jammed state. For the four post-liquefaction simulations, the percolation indexes are all smaller than 1 at the initial stages of shearing. The percolation indexes in the lateral directions (x and y) jump abruptly to approximately 1. The percolation index in the vertical (z) direction coinciding with loading also increases sharply to approximately 1 for samples with compressive residual axial strains (PL-1 and PL-3) but increases gradually to approximately 1 for samples with extensive residual strains (PL-2 and PL-4). This shows that, for the former cases, the sample states rapidly transition from unjammed to jammed, bypassing the fragile state, whereas a complete phase transformation process from an unjammed state to a fragile state and finally to a jammed state is observed for the latter cases. This is understandable: when the original strain is compressive, the existing major force transmission network is already compatible with further compressive straining and radical alternations of the force transmission network are not needed. However, when the original strain is extensive, the existing force transmission network is compatible with extensive loading and has to be rearranged to form a stable network that is adapted to the compressive loading. This requires a longer period of straining. In all four post-liquefaction cases, a fully percolated force transmission network is formed before the sample reaches the end of Phase I.

To better elucidate the evolution of the force transmission network and its relationship with the stress–strain response, the elementary particles comprising the largest force transmission networks at five characteristic loading stages of PL-2 (points A to E in Fig. 7(c)) are visualised in Fig. 8. The remaining clusters of particles are small in size and make much less contribution to sustaining the external loads than the major force network, and thus are not shown in Fig. 8 for clarity. The particles comprising the force transmission network are shaded according to their number of neighbouring particles. At the beginning of shearing (Fig. 8(a)), the largest force transmission network is a small group of particles clustered in the middle of the bottom rigid wall. It extends closely to the lateral cylindrical wall, but is far from percolation in the vertical direction. The cluster is sparsely packed as most of the particles contain fewer than 3 contacting neighbours. This cluster grows in both the lateral and vertical directions during loading. Note that the top rigid boundary is fixed and loading is achieved by moving the bottom rigid boundary upwards, which leads to a clear propagation of the force transmission network from bottom to top. The force network is further strengthened and includes more particles as loading further proceeds. Fig. 8(c) shows that when the force transmission network has just fully percolated, although as a whole it percolates in all directions, it does not extend to the lateral directions at its top 1/4 part. This localised fragile state makes the force transmission network remain vulnerable to variations of external loading and be unstable. Fig. 8(d) illustrates the force transmission network close to the end of Phase I. At this instant, the force transmission network percolates along the entire height and thus can continuously sustain the external loading, i.e., a reliable and robust force transmission network is formed. The force transmission network is further strengthened and the particles within the force transmission network are more closely packed as loading further proceeds (Fig. 8(e)). Fig. 8 indicates that percolation is a necessary but is not a sufficient condition for the formation of a stable and robust force transmission network. The force transmission network requires further strengthening before it can sustain external loading like a solid. Furthermore, it can be seen from Fig. 8 that the major force transmission network was mechanically unstable at the flow and fragile states but became increasingly stable after reaching the jammed state. This is consistent with Fig. 4(a) which showed that the axial strain

developed rapidly at loading Phase I but the development of axial strain slowed down in the subsequent loading phases.

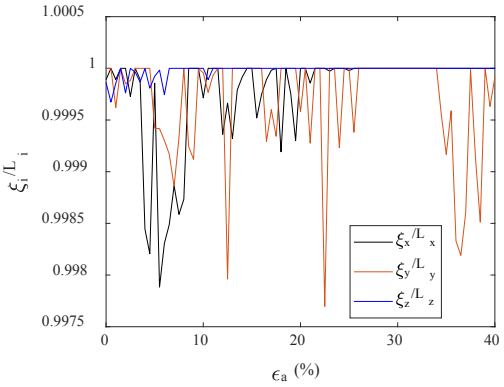

(a) Virgin sample

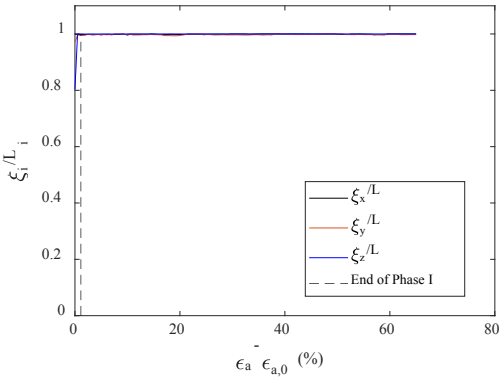

(b) Sample PL-1

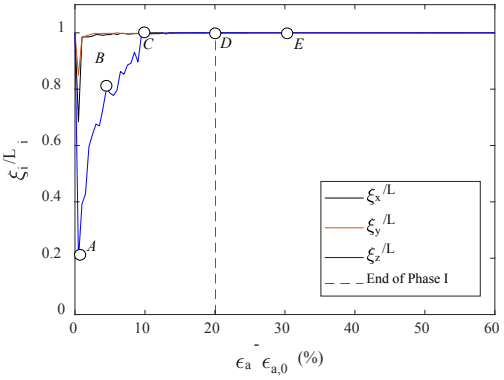

(c) Sample PL-2

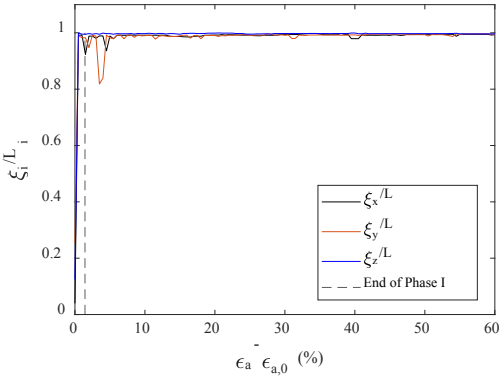

(d) Sample PL-3

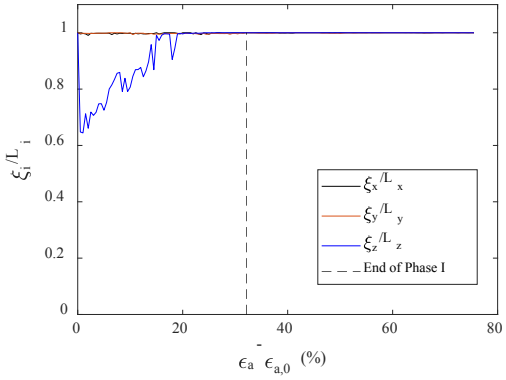

(e) Sample PL-4

Figure 7 Evolution of the percolation indexes during the monotonic constant-volume simulations

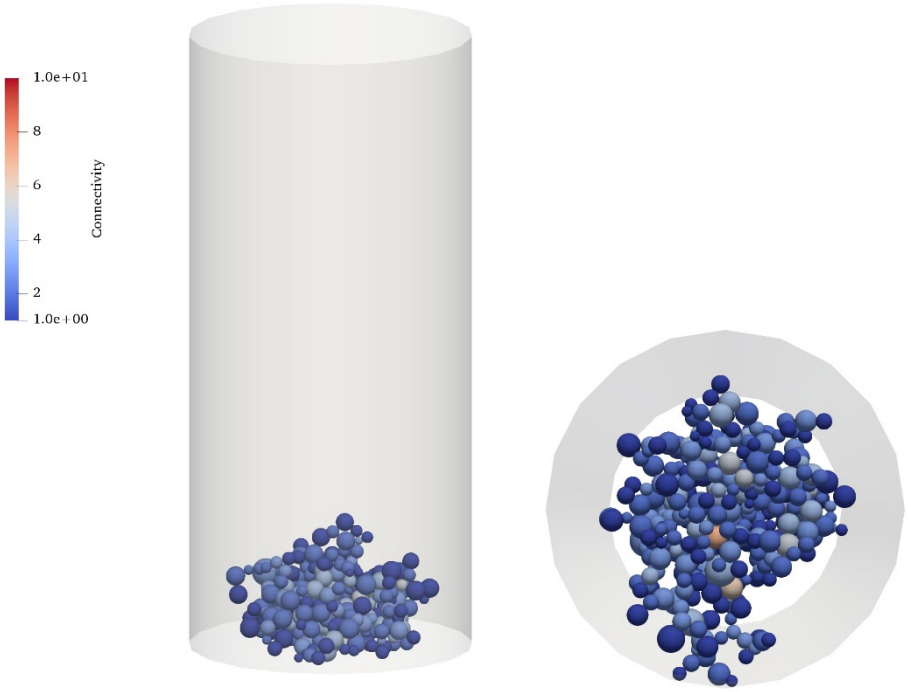

(a) instant A (ε_a-$\varepsilon_{a,0}$=0.5%)

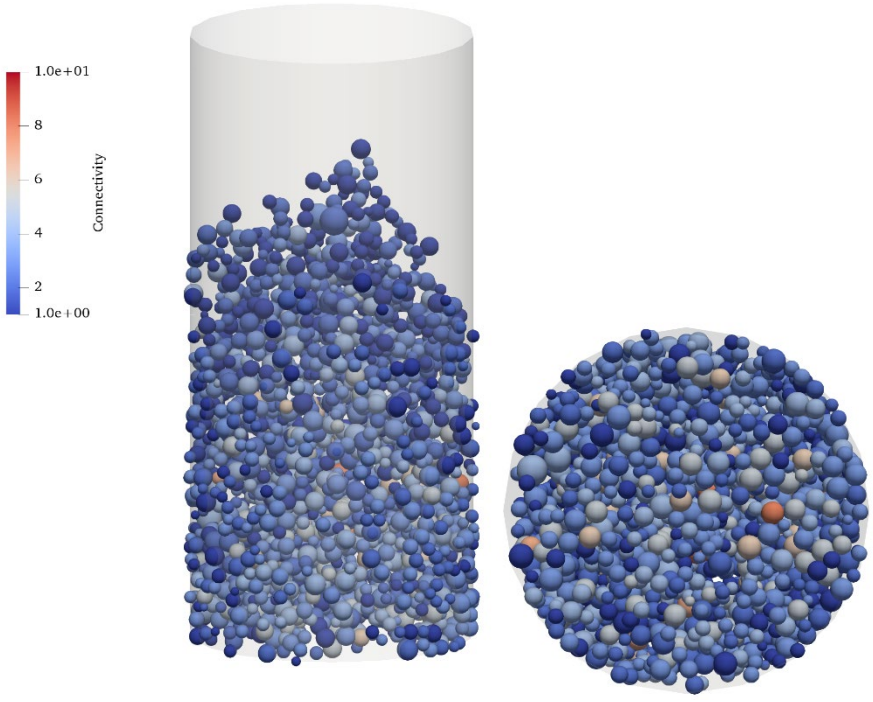

(b) instant B (ε_a-$\varepsilon_{a,0}$=5%)

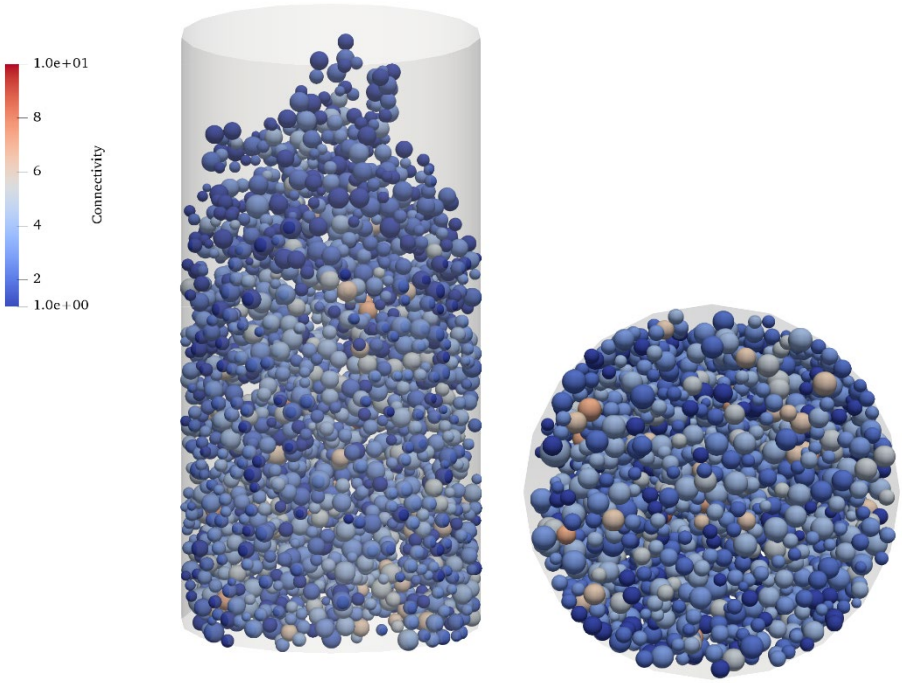

(c) instant C (ε_a-$\varepsilon_{a,0}$=10%)

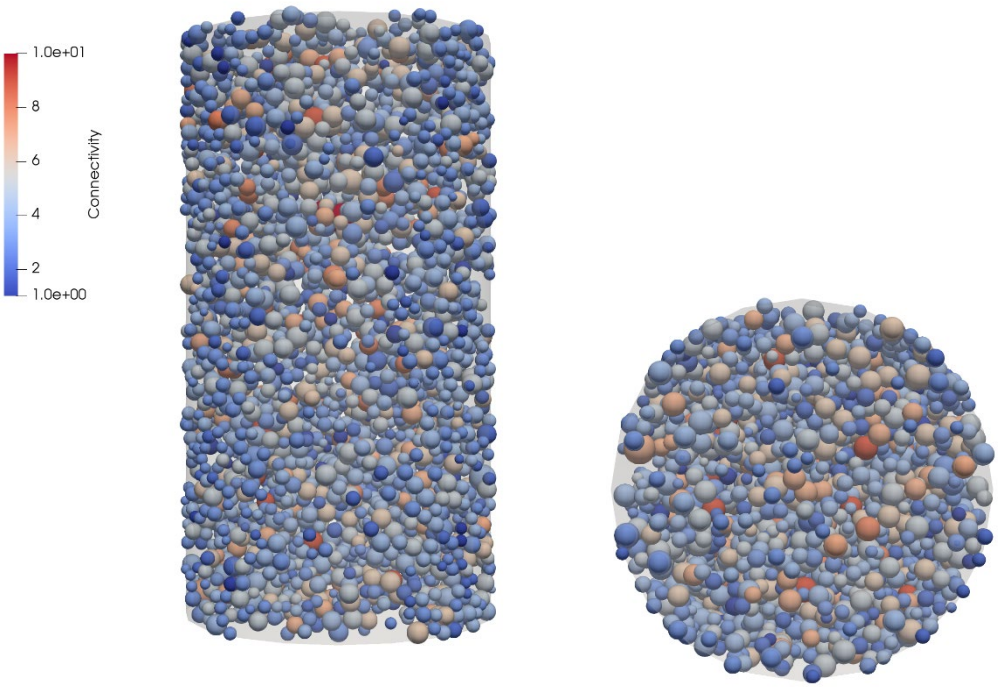

(d) instant D (ε_a-$\varepsilon_{a,0}$=20%)

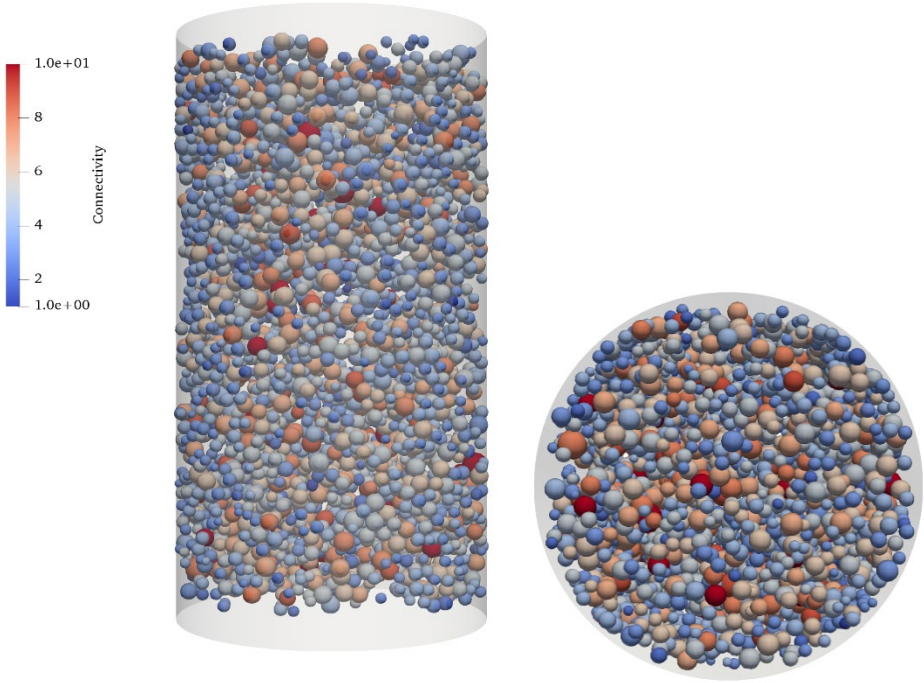

(e) instant E (ε_a-$\varepsilon_{a,0}$=31%)

Figure 8 Visualisation of particles in the largest force transmission network at different loading stages for the PL-2 simulation. The shaded colour of particles is scaled by the number of neighbouring particles

3.4 Resilience of force transmission network

Following the work of Herrera et al. [35] and Slotterback et al. [36], the resilience of the force transmission network is evaluated considering the size of the largest force transmission network (S_L), the number of clusters (N_{cl}) relative to the total number of particles (N_p) and the fraction of broken contacts (B_L). Two additional measures were also quantified: the mean size of clusters and the sliding fraction. Specifically, S_L is defined as ratio of the number of particles within the largest force transmission network to the total number of particles within the sample. N_{cl} is the number of groups of inter-connected particles. B_L is defined herein as the ratio between the number of broken contacts and the total number of contacts within the sample at the same loading instant. Note that, when calculating B_L, the required contact information is recorded regularly at an interval of 0.5% axial strain. The previous recording state is taken as the reference frame and the reformed contacts are also taken into account. In

this way, the number of broken contacts can be easily obtained by comparing the list of contact IDs at the current state with that at the reference state. The mean size of clusters is the average number of particles comprising a cluster, i.e., the total number of particles divided by N_{cl}.

Figure 9 compares the evolution of S_L for the virgin sample and the four liquefied samples during monotonic shearing. The vertical dashed lines mark the end of loading Phase I for the liquefied samples. It quantifies the size of the largest force transmission network relative to the overall sample. The larger S_L is, the more stable and resilient the force transmission network will be as there are multiple redundant paths for force transmission: failure of an individual connected particle column by buckling [37] can be compensated by other surrounding particles. In the virgin sample case, S_L decreases slightly at the beginning due to the change of loading mode from isotropic compression to triaxial shearing but it then increases as loading further proceeds. It is consistently higher than 0.8. For the four liquefied samples, S_L is small at the initial stages of loading (S_L values for PL-2 and PL-4 are close to 0) and surges sharply during Phase I of loading. At this stage, the particles rearrange substantially to form a percolated force transmission network (see Fig. 7). S_L continues to grow at a decreasing rate during Phases II and III and finally becomes more or less constant when the critical state is attained. At these stages, the major force transmission network is further strengthened due to the increase of stresses induced by dilation. As Fig. 9(f) shows, although S_L values for the five simulations differ significantly before approaching the critical state, they eventually converge and reach a identical value of around 0.88 at the critical state. Similar to the percolation anaysis, it requries more straining for the samples with initial extensive residual strains to form a stable force transmission network than the samples with initial compressive residual strains. The S_L values at the end of Phase I are close to 0.78 which, for this grading, may be the minimal size of force transmission network required for the sample to behave as a solid. To better illustrate this point, Fig. 10 plots S_L against the deviatoric stress q. For all of the four post-liquefaction simulations, the deviatoric stress is essentially zero and S_L surges up until S_L reaches 0.78. q then grows nonlinearly with S_L as S_L is further increased.

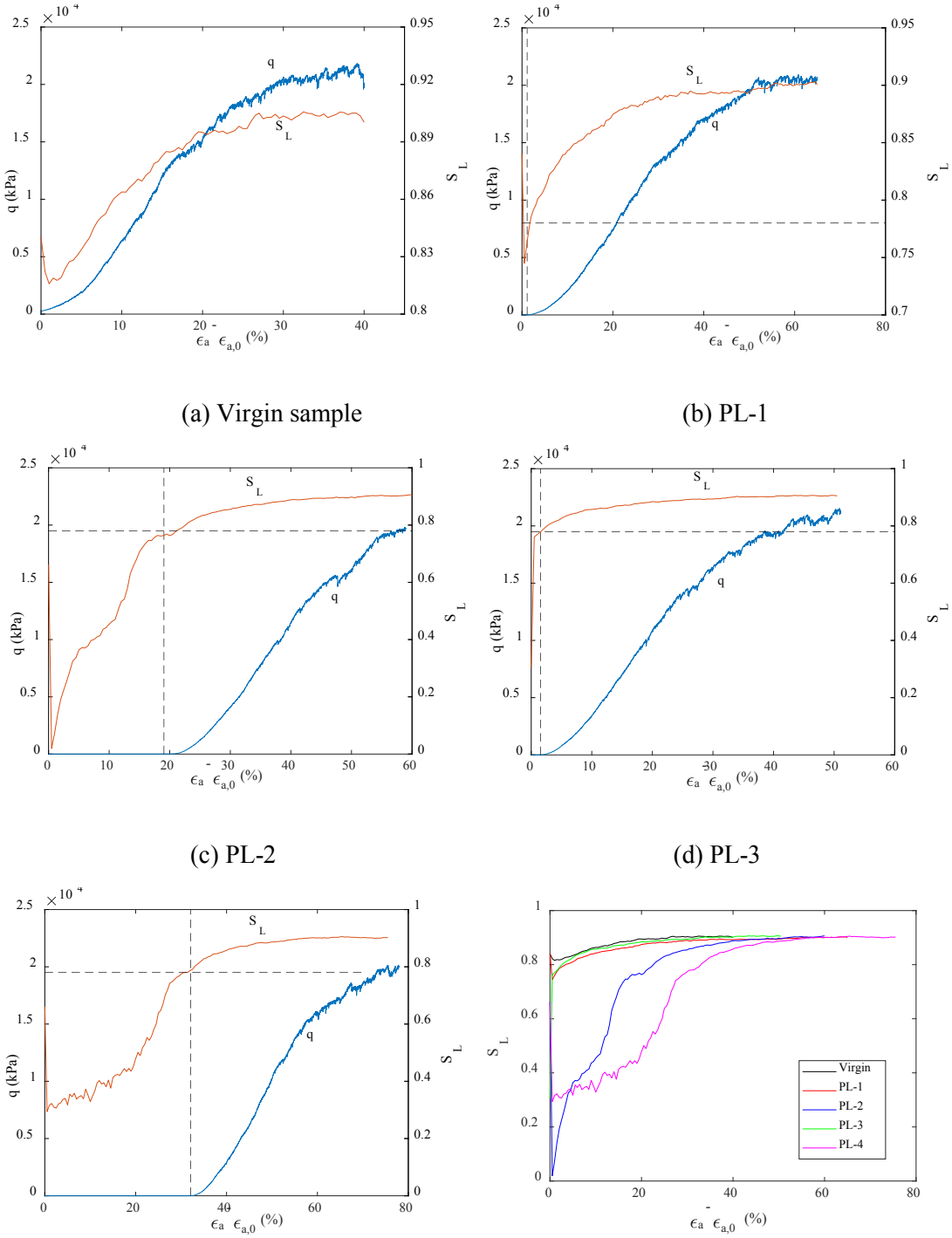

(a) Virgin sample

(b) PL-1

(c) PL-2

(d) PL-3

(e) PL-4

(f) together

Figure 9 Variation of size of the largest force transmission network (S_L) with the axial strain

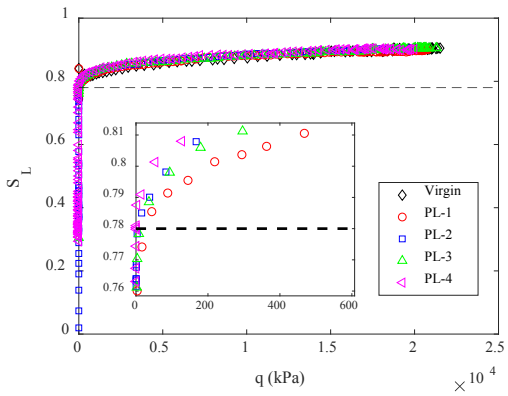

Figure 10 Variation of S_L with q

Fig. 11(a) shows the evolution of the number of clusters (N_{cl}) normalised by the total number of particles (N_p), i.e., N_{cl}/N_p, against axial strain. Isolated particles are also considered as clusters in this metric. The solid squares mark the instants when the end of loading Phase I is reached. A large N_{cl}/N_p value indicates a high degree of isolation of individual particles. As N_{cl}/N_p approaches 1, most particles become isolated with no contacting neighbours. Their movement will not be restricted by other particles and the system will flow like a liquid subjected to external disturbances. The N_{cl}/N_p value of the virgin sample remains below 0.2 throughout the simulation, which indicates that the particles within the virgin sample are well interconnected. The value increases slightly at the beginning of shearing but later decreases continuously until the critical state is reached. For the four liquefied samples, the N_{cl}/N_p values are all above 0.3 at the beginning of shearing. In particular, N_{cl}/N_p values for PL-2 and PL-4 are close to 1. The N_{cl}/N_p values for the liquefied samples decrease sharply at the loading stage of Phase I as small clusters merge to form more stable major force transmission networks (see Fig. 9). N_{cl}/N_p continues to decrease due to the strengthening of the major force transmission network as loading proceeds until an approximately constant value is reached at the critical state. In general, the change in N_{cl}/N_p values is more notable before reaching the end of loading Phase I than in the subsequent stages. Despite differences before approaching the critical state, all five curves converge to a value around 0.097 at the critical state regardless of the liquefaction history.

Fig. 11(b) shows the evolution of the mean size of clusters against axial strain. The mean size of clusters indicates the overall stability of the clusters. For the virgin sample, the mean size

of the clusters is about 6 at the initial stage of loading. It decreases slightly due to the change of loading mode from isotropic compression to triaxial shearing, and then increases gradually to an approximately constant value at the critical state. For the four liquefied samples, the mean sizes of the clusters are all below 4 before triaxial shearing is commenced. In particular, the mean sizes of clusters in PL-2 and PL-4 at the beginning of loading are close to 1, i.e., each cluster only contains one single particle. In such a case, the sample is essentially in a fluidic state. The mean size of clusters increases abruptly at the loading stage of Phase I owing to the increasing size of the largest force transmission network (Fig. 9) and decreasing number of clusters (Fig. 11(a)). They continue to increase at a decreasing rate and reach a more or less constant value at the critical state. Despite the liquefaction history, all samples reach an identical mean cluster size of 10 at the critical state.

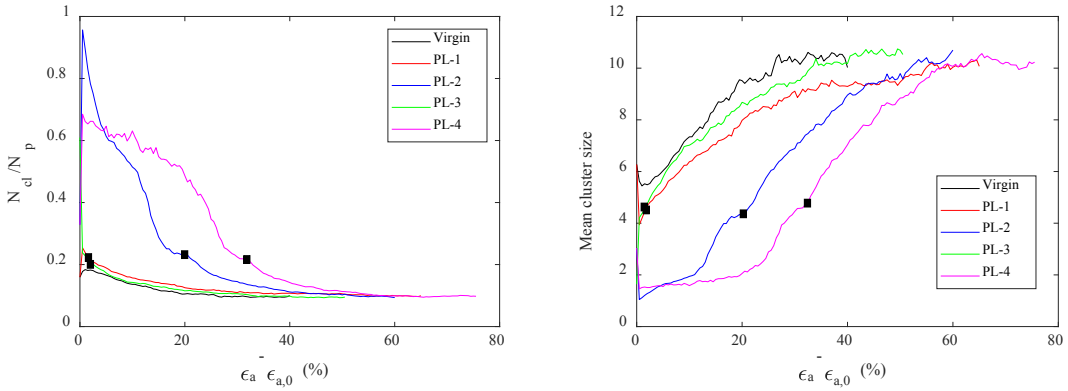

(a) (b)

Figure 11 Evolution of clusters during the simulations (solid squares mark the end of loading Phase I): (a) Number of clusters normalised by the total number of particles; (b) Mean size of clusters

As noted by Hanley et al. [38], contacts within a granular assembly are not constant but may experience a dynamic process of birth, separation and regeneration during shearing. The number of contact loss events during shearing reflects the stability of the overall force transmission network. Fig. 12 shows the evolution of the broken contact fraction (B_L) throughout the five simulations. For the virgin sample, B_L is 0.167 at the beginning of shearing and decreases continuously until an approximately constant value is reached at the critical state, i.e., the overall stability of the force transmission network increases

continuously during shearing. As noted by Pouragha and Wan [39] amongst others, when subjected to deviatoric loading, an initially jammed denser sample will experience more contact loss and gain events than an initially jammed looser sample as a consequence of structural optimisation and release of redundant contacts. The situation for liquefied samples which are initially unjammed is different. Subjected to external shearing, the force transmission network is gradually formed and percolates until the isostatic state (the number of contacts just meets the requirement of mechanical stability) is reached (Phase I behaviour). During this procedure, the coordination number, i.e., the total number of contacts, increases gradually (see Fig. 17). As a result, the stability of the force transmission network also increases accordingly. At this stage, contact variation is also associated with the stability of the force transmission network. For the four liquefied samples, the B_L values are very large at the beginning of shearing, which indicates dramatic contact rearrangements. B_L values for PL-2 and PL-4 are close to 1, which means all the contacts will be altered subjected to shearing and the resilience of the force transmission network is poor. B_L decreases sharply at the loading stage of Phase I as a stable force transmission network is gradually formed due to cluster coalescence and it continues to decrease at a decreasing rate as loading further proceeds. B_L approaches a value of about 0.03 at the critical state for all simulations.

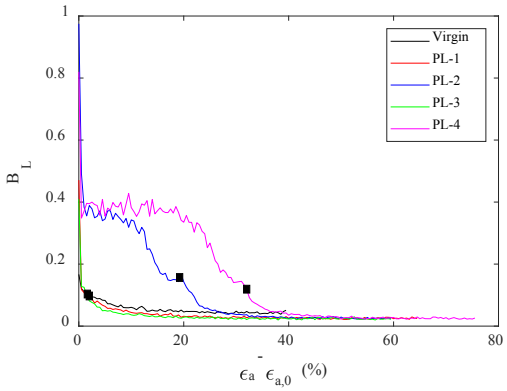

Figure 12 Evolution of the broken contact fraction during the simulations (solid squares mark the end of loading Phase I)

Contacts will slide in the tangential direction when the tangential contact force (f_t) reaches its plastic limit, i.e., the product of interparticle friction coefficient (μ) and the normal contact force (f_n). The stability of the force transmission network can be further investigated through

the analysis of the sliding fraction (f_s) which is defined as the number of contacts reaching the plastic limit in the tangential direction relative to the total number of contacts. Fig. 13 illustrates the evolution of sliding fraction during the five simulations. In the virgin sample case, the sliding fraction is about zero at the beginning of shearing. It increases sharply when loading is changed from isotropic compression to deviatoric shearing, but remains small (≈5%) throughout the simulation. For the liquefied samples, the sliding fractions all exceed 20% at the beginning of shearing and the sliding fractions of PL-2 and PL-4 are even larger than 40%, indicating dramatic particle rearrangements. The sliding fraction decreases sharply at the loading stage of Phase I as a percolated stable force transmission network is gradually formed and its resilience is gradually increased at this stage (see Fig. 7 to Fig. 9). Despite some oscillations, the sliding fraction, an indicator of the extent of particle rearrangement, becomes more or less constant in the subsequent stages of loading. All five simulations reach a constant sliding fraction of around 5% at the critical state. Although the stresses and volume will not change at the critical state, the sample's geometry continues to change, becoming shorter in the vertical direction and larger in the circumferential direction. Therefore, some contacts originally oriented in the vertical direction have to slide in order to adapt to the change of sample geometry, explaining why a small portion of sliding contacts are still present at the critical state. This also explains why some contact separation events continue to occur at the critical state as Fig. 12 shows.

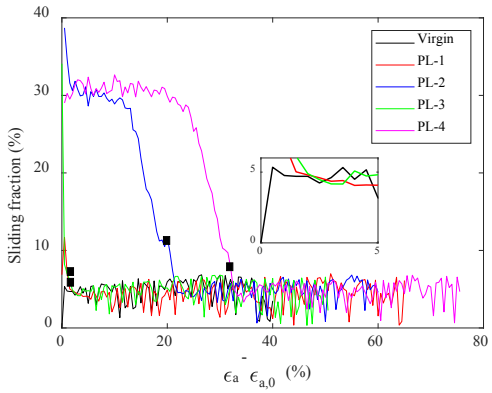

Figure 13 Evolution of sliding fraction during the simulations (solid squares mark the end of loading Phase I)

Fig. 9 to Fig. 13 show that, for the virgin sample, the resilience of the force transmission network is initially at a high level and is further strengthened during deviatoric shearing due to dilation-induced increase of stresses. However, for the liquefied samples, major particle rearrangements occur at the loading stage of Phase I until a stable major force transmission network is formed through cluster coalescence. The resilience of the force transmission network is further enhanced in the subsequent loading stages as small clusters merge with the major force transmission network. An identical degree of resilience is reached at the critical state regardless of the liquefaction history.

3.5 Mechanical redundancy

A mechanically stable granular system requires the total number of constraints provided by contacts to exceed the total number of degrees of freedom of particles. At the 'isostatic' state, the particles will have just enough contacts to maintain a rigid state, i.e., the total number of constraints should be equal to the total number of degrees of freedom. If the total number of constraints is above the isostatic value, the system is in a jammed state and will behave like a solid; otherwise, the system is in an unjammed state and will behave like a fluid [40]. The following two parameters are used herein to assess the mechanical stability of the sample during the simulations.

3.4.1 Index of mechanical redundancy

Kruyt and Rothenburg [41] proposed an index of redundancy (I_R^{NR}) to quantify the excessive constraints with respect to the total number of degrees of freedom within a granular system.

$$I_R^{NR} = \frac{(3-2f_s)N_c}{6(N_p-N_P^0)} \quad \text{(Eq. 3)}$$

where N_c is the total number of contacts, N_p is the total number of particles, and N_P^0 denotes the number of floating particles (rattlers) with zero contacts. From a structural mechanics perspective, Eq. 3 can also be viewed as the ratio between the total number of equilibrium equations and the total number of unknowns. If I_R^{NR} is greater than (indeterminate) or equal to (determinate) 1.0, the system is mechanically stable; otherwise, the system is mechanically unstable (variable). Fig. 14 shows the evolution of I_R^{NR} during shearing. The initial I_R^{NR}

values are 1.292, 0.954, 0.306, 0.439, 0.559 for the virgin sample, PL-1, PL-2, PL-3 and PL-4, respectively. This indicates that only the virgin sample is initially in a mechanically stable state. All of the liquefied samples are initially in a mechanically unstable state and thus flow at the initial stage of loading (see Fig. 4). For the virgin sample, I_R^{NR} decreases slightly due to the change of loading mode at the onset of shearing but increases thereafter due to the increase of stresses induced by dilation until an almost constant value is reached at the critical state. For the liquefied samples, I_R^{NR} increases sharply during the loading stage of Phase I and exceeds the critical value of 1.0 approximately at the end of the loading stage of Phase I. I_R^{NR} continues to increase during the subsequent loading stages until the critical state is reached. Regardless of the liquefaction history, all samples reach an identical I_R^{NR} value of about 1.26 at the critical state.

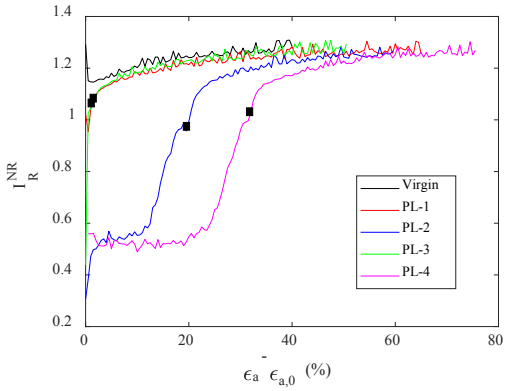

Figure 14 Evolution of mechanical redundancy (solid squares mark the end of loading Phase I)

Pouragha and Wan [19] used the difference between a modified version of I_R^{NR} and 1 to describe the degree of indeterminacy of a granular system. Fig. 15 shows the evolution of q against $I_R^{NR} - 1$ during the five simulations. The data points for all samples converge and can be conceptually divided into four zones: Zone 1 where the sample is variable as $I_R^{NR} - 1$ is negative and q is essentially zero ($I_R^{NR} - 1 < 0$); Zone 2 in which q starts to grow when the granular system becomes determinate ($I_R^{NR} - 1 = 0$ to 1.2), following a power law; Zone 3 in which q continues to grow in a linear manner as the degree of indeterminacy is further increased ($I_R^{NR} - 1 =$1.2 to 1.25); Zone 4 in which q increases more and more gradually and eventually becomes constant ($I_R^{NR} - 1 >$ 1.25).

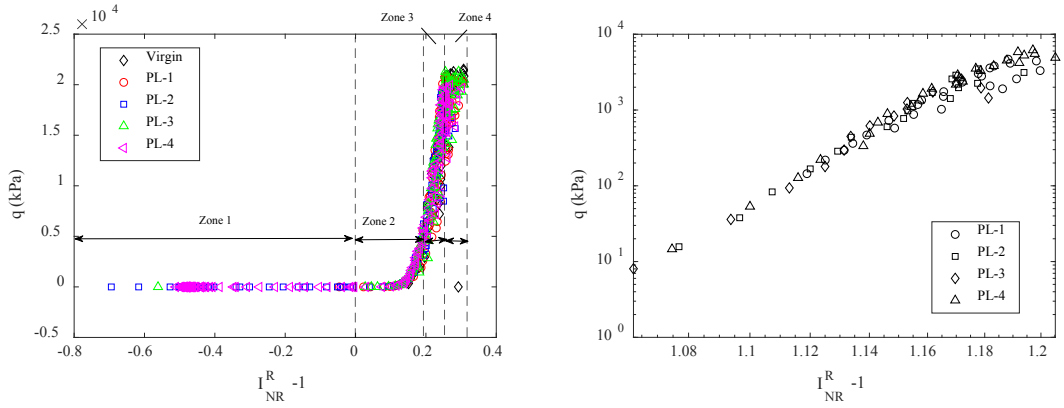

(a) all the data points (b) data points in zone 2

Figure 15 Relationship between q and the degree of indeterminacy

Figure 15 clearly shows that the strength of a granular system is closely related to the degree of indeterminacy regardless of the liquefaction history. Considering that the current approach of identifying different stages of post-liquefaction behaviour is quite subjective, Fig. 16 uses the $I_R^{NR} - 1$ values bounding different zones in Fig. 15 to separate the post-liquefaction stress-strain relationships. It is interesting to note that using this approach a flow stage, a non-linear stage, a linear stage and a stage approaching the critical state can be clearly identified for all of the four simulations. This indicates that the degree of indeterminacy can serve as an effective micro-scale index for the identification of different stages of post-liquefaction behaviour.

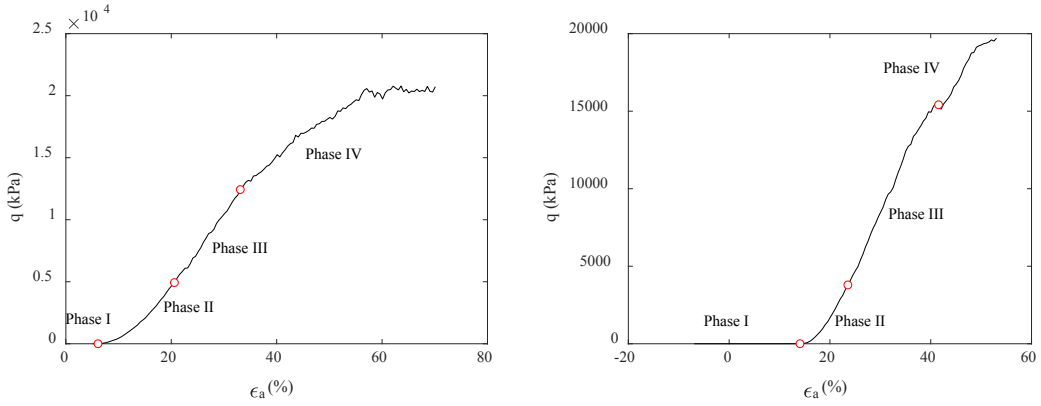

(a) PL-1 (b) PL-2

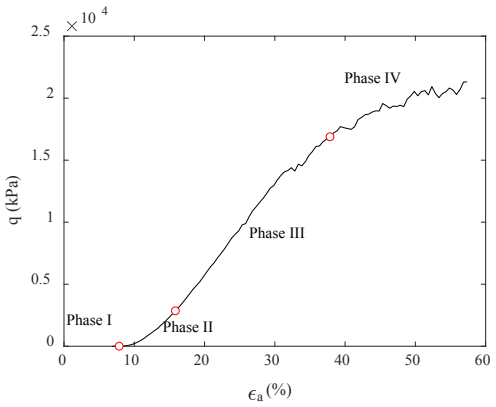

(c) PL-3

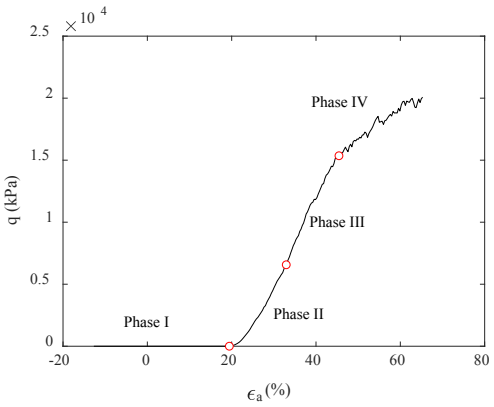

(d) PL-4

Figure 16 Identifying the different stages of post-liquefaction behaviour based on the degree of indeterminacy of the force transmission network (open circles mark the different characteristic degrees of indeterminacy)

3.3.2 Mechanical coordination number

Following Thornton [41], the mechanical coordination number (Z) is used to describe the average connectivity between particles:

$$Z = \frac{2N_c - N_p^1}{N_p - N_p^0 - N_p^1} \quad \text{(Eq. 4)}$$

in which N_c is the total number of contacts, N_p^0 and N_p^1 are the numbers of particles with 0 and 1 contacting particle, respectively.

For a frictional 3D system, we in total have $3 \cdot N_c$ (which can be converted to $3/2 \cdot Z \cdot N_p$) force degrees of freedom. We also have $6 \cdot N_p$ force and torque balance equations to solve these force degrees of freedom. For those sliding contacts with $f_t = \mu f_n$, the shear force is related to the normal force, which provides $f_s \cdot N_c$ additional constraints. Then we will have the following equation at the jamming transition instant: $3 \cdot N_c = 6 \cdot N_p + f_s \cdot N_c$, which leads to an isostatic Z_{iso} of Eq. 5 based on Eq. 4:

$$Z_{iso} = \frac{12}{3 - f_s} \quad \text{(Eq. 5)}$$

Z_{iso} is the lowest value of Z required to maintain the mechanical stability of a granular system in three dimensions. Theoretically, for a stable (jammed) system, Z should always be larger than Z_{iso}; otherwise, the system is mechanically unstable and will flow. A granular system is essentially unjammed if Z is smaller than Z_{iso}; it is at the unjamming–jamming transition state when Z equals to Z_{iso}, and is in a hyperstatic state if Z is larger than Z_{iso}. The difference between Z and Z_{iso} can be used to describe the distance of a granular system from an isostatic state.

Fig. 17 compares the evolution of Z (solid lines) and Z_{iso} (dashed lines) during the five simulations. The initial Z values are 4.86, 4.07, 3.54, 2.76 and 3.5 for the virgin sample, PL-1, PL-2, PL-3 and PL-4, respectively, whereas the initial Z_{iso} values are 4.00, 4.09, 4.59, 5.18 and 4.28, respectively. Only the virgin sample has a Z value that is larger than Z_{iso}, which indicates that only the virgin sample is initially mechanically stable and in a solid state, whereas the liquefied samples are initially mechanically unstable and can flow. Z increases but Z_{iso} decreases sharply during the loading stage of Phase I due to the reduction of sliding fraction (see Fig. 13). Z and Z_{iso} cross over each other at the transition points between the loading stages of Phase I and Phase II, after which Z continues to grow until a constant value is reached at the critical state. Z_{iso} becomes constant immediately after the loading stage of Phase I. A constant Z value of approximately 5 and a constant Z_{iso} value oscillating between 4.0 and 4.1 are reached at the critical state for all the simulations regardless of their liquefaction history.

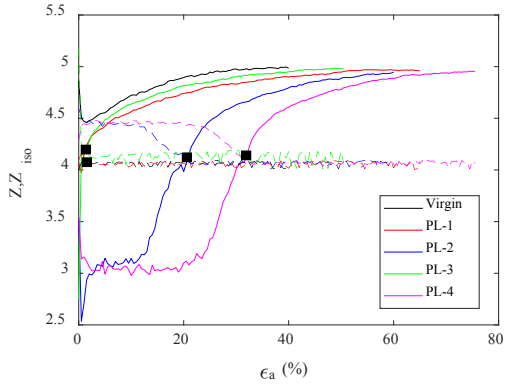

Figure 17 Evolution of the mechanical and isostatic coordination numbers (solid squares mark the end of loading Phase I, solid lines are calculated Z and dashed lines are the minimum Z values required to maintain the overall stability of the sample)

Fig. 14 to Fig. 17 clearly show that the virgin sample is consistently in a mechanically stable (jammed) state but the liquefied samples are initially in a mechanically unstable (unjammed) state and become mechanically stable (jammed) after the loading stage of Phase I. This is the physical explanation why the virgin sample behaves consistently similar to a solid but the liquefied samples flow at the beginning of shearing before regaining strength and stiffness.

4 Conclusions

A series of monotonic constant-volume triaxial simulations were performed on liquefied samples having different residual strains. These samples were selected at different liquefaction instants of a stress-controlled constant-volume cyclic loading simulation on an isotropic virgin sample. For comparison, a monotonic constant-volume triaxial simulation was also carried out on the virgin sample. The simulation results showed that the virgin sample behaved dilatively throughout the simulation, while the stress–strain behaviour of the liquefied samples could be divided into four phases that have been well documented in the experimental literature, i.e., flow (Phase I), regaining of strength and stiffness at increasing rates (Phase II), further increase of strength at a constant stiffness (Phase III) and approaching the critical state (Phase IV). The stress–strain curves of all the simulations converge eventually, indicating an identical critical state that is independent of the liquefaction history.

The fundamental mechanism underlying the aforementioned macro-scale mechanical behaviour is linked to the jamming concept considering percolation of the force transmission network, resilience of the force transmission network and mechanical redundancy. It is shown that the virgin sample is consistently in a jammed state during shearing, characterised by a fully percolated force transmission network. This force transmission network comprises a large portion of the particles within the sample and is resilient, with few contact loss events when subjected to external shearing. It is also mechanically stable with excessive constraints provided by the contacts to the particles. For the liquefied samples, the transition from

unjammed to jammed states during shearing is obviously observed. The force transmission network does not percolate in any dimension at the onset of shearing. However, it extends rapidly in all three dimensions through the coalescence of small clusters and finally becomes fully percolated at the end of the loading stage of Phase I. During this process, its resilience increases and its mechanical stability also increases sharply until the coordination number and the index of redundancy reach their isostatic values. Percolation of the force transmission network does not indicate that the sample will behave like a solid. A stable force transmission network requires its resilience and mechanical stability to reach a certain level. The intermediate fragile state is not obvious for samples with an initial compressive residual strain after liquefaction, but a successive unjammed–fragile–jammed phase transition is clear for samples originally experiencing an extensive residual strain. The resilience of the force transmission network continues to grow as loading further proceeds, as does the mechanical redundancy. In other words, the liquefied samples are in an unjammed state at the loading stage of Phase I but become jammed at the subsequent loading stages. In line with the macro stress–strain responses, all the micro-scale parameters converge at the critical state regardless of the liquefaction history. The recovery process of strength and stiffness for liquefied sands is physically a progressive evolution of the force transmission network from unjammed to jammed states followed by further strengthening until the critical state is reached.

The degree of indeterminacy is found to have a close relationship with the development of strength. A micro-scale approach is thereby proposed to identify different phases of post-liquefaction behaviour based on the degree of indeterminacy, which is shown to be able to clearly distinguish the four typical phases of post-liquefaction behaviour.

The observations made in this study will shed light on understanding the fundamental mechanisms underlying the influence of liquefaction on the mechanical behaviour of sands.

Acknowledgement

This research is funded by the National Natural Science Foundation of China (No. 51509186).

References

[1] Ishihara, K. Liquefaction and flow failure during earthquakes. Géotechnique 1993; 43(3): 351–415.

[2] Porcino, D., Caridi, G. Pre- and post-liquefaction response of sand in cyclic simple shear. Geotechnical Special Publication 2007; (160): 1-10.

[3] Seed, R. B., Harder, L. F. SPT-based analysis of cyclic pore pressure generation and undrained residual strength. Proceedings of H.B. Seed Memorial Symposium, J. M. Duncan, edited., BiTech, Richmond, BC, Canada; 1990, p. 351–376.

[4] Vaid, Y. P., Thomas, J. Liquefaction and post liquefaction behavior of sand. Journal of Geotechnical Engineering 1995; 121(2): 163–173.

[5] Shamoto, Y., Min-Zhang, J., Goto, S. Mechanism of large post-liquefaction deformation in saturated sand. Soils and Foundations 1997; 37(2): 71–80.

[6] Kokusho, T., Hara, T., Hiraoka, R. Undrained shear strength of granular soils with different particle gradations. Journal of Geotechnical and Geoenvironmental Engineering 2004; 130(6): 621–629.

[7] Sitharam,T.G., Vinod, J. S., Ravishankar, B.V. Post-liquefaction undrained monotonic behavior of sands: Experiments and DEM simulations. Géotechnique 2009; 59(9): 739–749.

[8] Sivathayalan, S., Mehrabi Yazdi, A. Influence of strain history on postliquefaction deformation characteristics of sands. Journal of Geotechnical and Geoenvironmental Engineering 2014; 140(3): 04013019.

[9] Schofield, A. N., Wroth, C. P. Critical State Soil Mechanics. McGraw-Hill; 1968.

[10] Finn, W. D. L., Yogendrakumar, M., Yoshida, N. Response of 2-D embankment systems to seismic loading, Soil mechanics series, Univ. of British Columbia, Vancouver, BC, Canada; 2009.

[11] Hamada, M., Towhata, I., Yasuda, S., Isoyama, R. Study on permanent ground displacement induced by seismic liquefaction. Computers and Geotechnics 1987; 4(4): 197–220.

[12] Elgamal, A., Yang, Z., Parra, E. Computational modeling of cyclic mobility and post liquefaction site response. International Journal of Soil Dynamics and Earthquake Engineering 2002; 22(4): 259–271.

[13] Liu, A. J., Nagel, S.R. Jamming is not just cool any more. Nature 1998; 21(6706): 21-22.

[14] Zhang, H. P., Makse, H. A. (2005). Jamming transition in emulsions and granular materials. Physical Review E 2005; 72(1): 011301.

[15] Liu, A., Nagel, S. The jamming transition and the marginally jammed solid. Annual Review of Condensed Matter Physics 2010; 1: 347-369.

[16] Bi, D., Zhang, J., Chakraborty, B., Behringer, R.P. Jamming by shear. Nature 2011; 480: 355-358.

[17] Kumar, N., Luding, S. Memory of jamming–multiscale models for soft and granular matter. Granular Matter 2016; 18(3): 1-21.

[18] Cates, M. E., Wittmer, J. P., Bouchaud, J. P., and Claudin, P. Jamming, force chains, and fragile matter. Physical Review Letters 1998; 81(9): 1841-1844.

[19] Pouragha, M., Wan, R. Onset of structural evolution in granular materials as a redundancy problem. Granular Matter 2016; 18(3): 38.

[20] Cundall, P.A., Strack, O.D.L.. A discrete numerical model for granular assemblies. Géotechnique 1979; 29 (1): 47–65.

[21] O'Sullivan, C. Particle-Based Discrete Element Modeling: Geomechanics Perspective. International Journal of Geomechanics 2011; 11(6): 449–464.

[22] Barreto, D., O'Sullivan C. The influence of inter-particle friction and the intermediate stress ratio on soil response under generalised stress conditions. Granular Matter 2012; 14(4): 505-521.

[23] Guo, N., Zhao J.D. The signature of shear-induced anisotropy in granular media. Computers and Geotechnics 2013; 47: 1-15.

[24] Gu, X.Q., Huang, M.S., Qian, J.G. DEM investigation on the evolution of microstructure in granular soils under shearing. Granular Matter 2014; 16(1): 91-106.

[25] Huang, X., O'Sullivan, C., Hanley, K. J., Kwok, C. Y. Discrete-element method analysis of the state parameter. Géotechnique 2014; 64(12): 954-965.

[26] Kuhn, M.R., Renken, H.E., Mixsell, A.D., Kramer, S.L. Investigation of Cyclic Liquefaction with Discrete Element Simulations. Journal of Geotechnical and Geoenvironmental Engineering 2014; 140(12): 1-13.

[27] Xu, X.M., Ling, D.S., Cheng, Y.P., Chen, Y.M. Correlation between liquefaction resistance and shear wave velocity of granular soils: a micromechanical perspective. Géotechnique 2015; 65(5): 337-348

[28] Ning, Z.W., Khoubani, A., Evans, T.M. Particulate modeling of cementation effects on small and large strain behaviors in granular material, Granular Matter 2017; 19: 7.

[29] Wang, G., Wei, J.T. Microstructure evolution of granular soils in cyclic mobility and post-liquefaction process. Granular Matter 2016; 18(3): 1-13.

[30] Wei, J.T., Huang, D.R., Wang, G. Microscale descriptors for particle-void distribution and jamming transition in pre- and post-liquefaction of granular soils. Journal of Engineering Mechanics 2018; 144(8): 04018067

[31] Itasca Consulting Group. Particle Flow Code in Three Dimensions: User's Manual, Version 4.0. Minneapolis, USA 2007.

[32] Hanley, K.J., O'Sullivan, C., Huang, X. Particle-scale mechanics of sand crushing in compression and shearing using DEM. Soils and Foundations 2015; 55(5): 1100-1112

[33] da Cruz, F., Emam, S., Prochnow, M., Roux, J. N., Chevoir, F. Rheophysics of dense granular materials: discrete simulation of plane shear flows. Physical Review E 2005; 72(2): 021309

[34] Lopera Perez J C , Kwok C Y , O"Sullivan C , et al. Exploring the micro-mechanics of triaxial instability in granular materials. Géotechnique 2016; 66(9):725-740.

[35] Herrera M., McCarthy S., Slotterback S., Cephas E., Losert W., Girvan M. Path to fracture in granular flows: Dynamics of contact networks. Physical Review E 2011; 83: 061303.

[36] Slotterback S., Mailman M., Ronaszegi K., van Hecke M., Girvan M., Losert W. Onset of irreversibility in cyclic shear of granular packings. Physical Review E 2012; 85: 021309.

[37] Tordesillas, A. Force chain buckling, unjamming transitions and shear banding in dense granular assemblies. Philosophical Magazine 2007; 87(32): 4987-5016.

[38] Hanley, K.J., Huang, X., O'Sullivan, C., Kwok, F. C.-Y. Temporal variation of contact networks in granular materials. Granular Matter 2014; 16(1): 41–54.

[39] Pouragha, M., Wan, R.. Non-dissipative structural evolutions in granular materials within the small strain range. International Journal of Solids and Structures 2017; 110-111: 94-105.

[40] Heussinger, C., Barrat, J. L. Jamming transition as probed by quasistatic shear flow. Physical Review Letters 2012; 102(21): 218303.

[41] Kruyt, N.P., Rothenburg, L. Plasticity of Granular Materials: a Structural-mechanics View. AIP Conference Proceedings 2009; 1145(1): 1073.

[42] Thornton, C. Numerical simulations of deviatoric shear deformation of granular media. Géotechnique 2000; 50(1): 43–53.